

# Study of salt fog phenomenon on the surface of excavated pottery sherds

Elshaimaa Abd Elrahim and Hamdy Mohamed Mohamed\*

Conservation Department, Faculty of Archaeology, Cairo University, 12613 Giza, Egypt

The phenomenon of salt fog on pottery surfaces attracted our team to study it and explain the reason for its formation. The crystallization of salts during drying leads to pottery damage. A significant step is to examine the types of salt and identify the chemical composition of the sherds. For this visual assessment, a digital microscope and a scanning electron microscope with energy dispersive X-ray analyses unit (SEM-EDX) were used to detect surface deterioration. In addition, X-ray diffraction (XRD) and Fourier transform infrared spectroscopy (FTIR) analyses were carried out to determine the chemical composition of potsherds and salts. The microscopic examination revealed a dense distribution of salts on the potsherd surface. Besides, the SEM photomicrographs showed clear cubic salt crystals of sodium chloride, especially after drying. The SEM-EDX analysis also revealed high chloride salt concentration, in addition to silica and aluminum oxide, which are the primary ingredients in pottery-making. According to XRD analysis, the pottery samples primarily contained diopside, hematite, magnetite, albite and muscovite, which are the primary components in manufacturing. Furthermore, halite appeared in large proportions due to the influence of burial soil. Besides, the quartz, clay minerals, hematite and calcite content of the samples were confirmed by FTIR. The results thus support the fact that sodium chloride significantly influences archaeological pottery.

**Keywords:** Archaeological pottery, salt efflorescence, sherds, sodium chloride, surface deterioration.

ARCHAEOLOGICAL pottery is historically significant because it provides information that helps historians understand ancient cultures<sup>1</sup>. Furthermore, pottery can be used together with more information about the location, the people interred there, and the significant religious practices of their descendants who came to the site in later centuries<sup>2</sup>. Several potsherds from the New Kingdom period in Egypt were discovered in 2020 at the Saqqara excavation site by researchers from the Faculty of Archeology, Cairo University, Egypt. For thousands of years, Saqqara has held great historical and cultural significance. Pottery is the most frequently discovered artifact during excavations<sup>3</sup>. The New Kingdom was a time of widespread prosperity, as reflected in

the pottery industry. Moreover, the pottery of this period was well made<sup>4</sup>.

Water indirectly affects artefacts like pottery by transporting soluble salts, one of the primary causes of artefact deterioration<sup>5</sup>. As water penetrates the pores, the pottery deteriorates due to salts, particularly soluble salts<sup>6</sup>. The most common cause of salt attack is increased moisture in the soil<sup>7</sup>. Therefore, water penetration into archaeological objects is considered the primary cause of degradation, especially in porous materials<sup>8</sup>. When salt is dissolved in water, it can be transferred through a porous substance. During surface drying, crystallizing and accumulating salt is transferred to the evaporation destination<sup>9</sup>. Temperature plays a significant role in the crystallization of soluble salts. Salts crystallize more rapidly at higher temperatures, whether inside the body or on an external surface<sup>10</sup>.

Salt crystallization in porous materials is a common cause of damage to archaeological objects<sup>9</sup>. Porosity has a vital role in the deterioration of archaeological pottery because the pore network permits penetration of water, which is accountable for the various chemical and physical damages in the pottery body<sup>11</sup>. Salt significantly affects the durability of archaeological pottery. Therefore, it is critical to comprehend the crystallization process inside the pottery body. This will help formulate a strategy to prevent or limit harm to porous materials<sup>12</sup>.

Soluble salts severely decrease the durability of porous materials. Consequently, preventing salt crystallization requires understanding the mechanisms that cause the same<sup>13</sup>. The penetration of salt solution into the interior pores of pottery generates fissures, while the crystallization of these salts on the exterior surface causes the surface decorations to be distorted<sup>14</sup>. The most popular theory proposes that when water evaporates, or temperature rises, the saline solution spreads inside the pores, where salt efflorescence begins. The permeability and pore size of the pottery, as well as the ambient temperature and relative humidity, impact the evaporation rate<sup>15</sup>.

The type and concentration of salts found on pottery surfaces vary widely, depending on the kind of pottery and the location where it is found<sup>16</sup>. However, salt fog activities also include the crystallization and deposition of salt fog on the surface of these objects. Potsherd pores become voids because of salt expansion after salt solution seeps into the pores<sup>17</sup>. The pore structure and saturation level influence the degree of crystallization in porous materials.

\*For correspondence. (e-mail: hamdy.mohamed@cu.edu.eg)

The pressure of crystallization is known to be lower in larger pores. Furthermore, high saturation levels result in high crystallization pressure. Salt crystallization primarily occurs on the porous surface of the pottery (efflorescence)<sup>13</sup>. Several factors influence the degree of saturation, including the initial solution concentration, relative humidity, temperature, substrate roughness and surface area<sup>18</sup>.

This research focuses on the impact of a salt solution on pottery sherds that results in the formation of salt crystals on their surface shortly after extraction from the Saqqara excavations. To understand why salt crystallizes and how quickly water evaporates in partial crystallization, it was necessary to explain how salt crystallizes and dissolves. Despite sodium chloride has been extensively studied for various applications, its crystallization mechanism still needs fully understood. Studies on this phenomenon are rare, and this interaction's physical and mechanical deterioration is poorly known. Excavated surroundings negatively affect archaeological findings through physical or chemical processes based on material properties. The present study aims to analyse this strange phenomenon, which appears on the surface of excavated pottery and damages the same, in addition to determining the influence of salt precipitation on the porous structure of the pottery. Understanding how salt crystallization affects the deterioration of porous pottery is critical for cultural heritage preservation.

## Materials and methods

### Materials

Two potsherds were chosen from the excavations at Saqqara to study the damage mechanism and determine the role of salts in the deterioration. The excavated sherds varied in size from small to large. The potsherds were coded to facilitate the discussion (Table 1).

### Methods of analysis

**Visual assessment:** The sample surfaces were examined using a camera (SONY) (16 megapixels CMOS beam, 8× optical zoom, up to clear 16× picture zoom, 25 mm wide-angle lens (35 mm format) and full HD movie (1920\*1080)).

**Table 1.** Description of potsherds

Code sample	Description
P1	A reddish-brown potsherd that is 1.1 cm thick, 22.4 cm long and 8.8 cm wide. It displays high crystallization of salts on the surface.
P2	A dark brown potsherd that is 1.4 cm thick, 9.6 cm long and 7.3 cm wide. It has a dry layer of salt droplets on the surface.

**Digital microscope:** The digital microscope utilized in the study had the following features: a high-definition CMOS sensor with a 5× digital zoom, a high-speed DSP (drive free offered), a 24-bit DSP, compatibility with both USB 3.0 and USB 2.0, and the ability to achieve super-resolution ranging from 640\*480 to 1600\*1200.

**Scanning electron microscope with elemental analysis unit (SEM-EDX):** The properties of the digital microscope instrument: using SEM Model Quanta 250 Field Emission Gun (FEG) attached with EDX Unit (Energy Dispersive X-ray analyzes), with accelerating voltage 30 KV, magnification 14× up to 1,000,000 and resolutions for Gun.1n), FEI Company, Netherlands.

**X-ray diffraction:** Cu-radiation ( $\lambda = 1.542 \text{ \AA}$ ) was used with a secondary monochromator on a PANalytical X-ray diffraction equipment (model XPert PRO at 45 kV, 35 mA and scanning speed of  $0.04^\circ/\text{sec}$ ). The relative intensities ( $I/I^\circ$ ), corresponding spacings ( $d$ ,  $\text{\AA}$ ), and diffraction peaks were measured between  $2\theta = 2^\circ$  and  $60^\circ$ . Diffraction charts and relative intensities are collected and compared with ICDD data.

**Fourier transform infrared spectroscopy (FTIR):** A FTIR spectrometer (Nicolet 380, Madison, WI, USA) was used to analyse the pottery samples employing the solid-sample potassium bromide technique with a resolution of  $4 \text{ cm}^{-1}$  ranging from 400 to  $4000 \text{ cm}^{-1}$ . The computer program Spectrum One was used to perform additional processing on the obtained FTIR spectra (ver. 5.0.1).

## Results and discussion

### Visual assessment

The chosen excavated potsherds were studied by the naked eye, in addition to using magnifying lenses (10×–20×) to determine the surface features, a dried crystal of saline solution on the excavated pottery sherds, and the appearance of its texture. Other aspects of deterioration were determined by observation and visual assessment. For example, morphologies of sodium chloride salts can be identified on the surface of the potsherds<sup>17</sup>. The type of material surface and solution saturation level both impact the crystallization behaviour of salts. Salt crystals and bristly efflorescence were observed on the surface of the potsherds. In the case of bristly efflorescence, crystals are formed inside the pores and grow outwards to the surface. The crystal stresses the surrounding material during this process, causing spalling and material loss<sup>7</sup>.

Due to the quick evaporation of salt-bearing water, the salt crystallizes rapidly on the surface of the potsherds<sup>19</sup>. Salt decay is generally considered a temperature/humidity-dependent weathering process caused by salt crystals on

the surface of the porous material. These crystals are typically visible<sup>20</sup>. The precipitation of solid particles from supersaturated liquid solution is a key step in the crystallization process. The main catalyst for crystallization from the solution is the difference in chemical potential between the solution and the solid phase<sup>18</sup>. In the present case, there were unclear water drops that had formed on the surface of the potsherds. The drops remained on the surface of the excavated pottery for 3–4 h after excavation and exposure to the environment. Then, they gradually dried out and disappeared, leaving behind small distorted spots or solid protrusions on the surfaces and in the pores (Figure 1).

### Digital microscope

One of the most important tools available to conservators is the digital microscope, whose images help assess the level of deterioration of an object<sup>21</sup>. Figure 2 *a* shows the presence of salt on the pottery surface in the form of cohesive crusts overlapping with the pottery body. Besides, a clear,

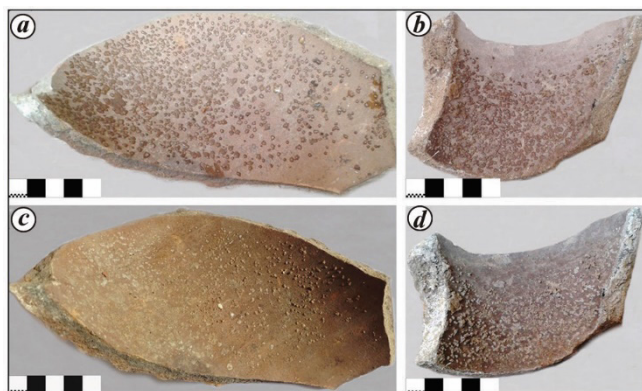


**Figure 1.** Potsherd samples before and after drying of saline solution. (*a, c*) Sample P1 and (*b, d*) sample P2.

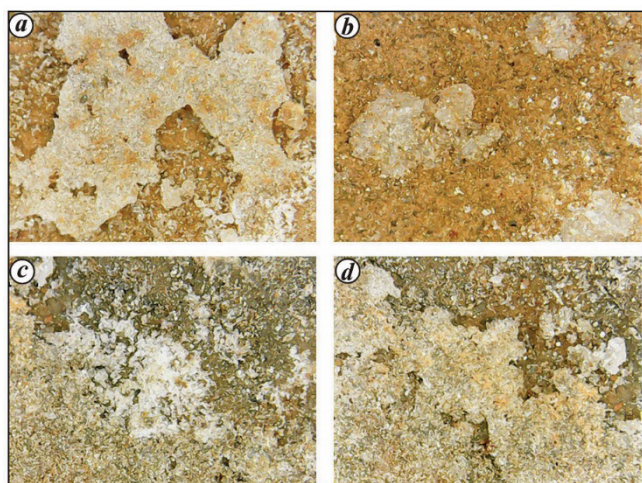


**Figure 2.** Salt crystallization on the potsherds. (*a, b*) Sample P1 and (*c, d*) sample P2.

dried, salt crystal layer covers the surfaces of the shred, penetrating inside and helping expand the size of the internal pores, which causes increased fragility of the pottery. In addition, salt efflorescence on the entire degraded surface is rough. Figure 2 *b* shows salt crystals arranged as cluster on the surface with a relatively substantial thickness. The salt crystal is obtained when the supersaturation indicating the beginning of crystallization is reached within the sherds<sup>22</sup>.

Figure 2 *c* and *d* shows a dense spread of salt on the surface of the potsherd and an overlap between the layers of salt, dust and sand scattered on the surface. Repeated salt crystallization and dissolution cycles in the pores influenced the pottery to crack and crumble. In the potsherds, efflorescence caused by salt deposits has been observed, resulting in detrimental degradation such as exfoliation and fragmentation<sup>7</sup>. If the rate of evaporation is greater than the supply rate of the solution, crystallization occurs on the surface of the pottery, resulting in salt efflorescence. This explains why salt crystals are found on the surface of the pottery<sup>15</sup>. Salt crystallization inside the pores of the pottery can produce enough stress to develop cracks in its body<sup>23</sup>.

### SEM

SEM is considered to be one of the most popular techniques for studying the morphology of pottery<sup>23</sup>. In the present study, SEM photo shows halite precipitates on the pottery surface with an equal distribution in a sample (P1). According to SEM analysis, salts form at or close to the surface because the dense crystalline structure inside the pottery prevents water and vapour transport<sup>19</sup>. If the evaporation rate is higher than the supply rate of the solution, salts are deposited inside the pores of the body. In this case, high crystallization occurs on the outer surface due to rapid water evaporation and the high temperature of the surrounding medium<sup>15</sup>. Due to salt in-filling pores, porosity decreases near the surface. Granular disaggregation and salt crystallization have been noticed at a depth of around 1 cm. The size of the interior pores determines the capacity of the saline solution to permeate the potsherds. The greater the pore size, the greater the penetration of the saline solution. On the other hand, the smaller the pore size, the less the penetration of the solution into the interior<sup>19</sup> (Figure 3).

In contrast, SEM images of sample P2 reveal clear cubic salt crystals of sodium chloride, especially after drying, as observed on the sample surface due to relative humidity (RH) evaporation and rise in temperature<sup>18</sup>. The shape of the salt crystal depends on various factors such as the evaporation rate and the porosity degree of the pottery. Cubic crystals will grow if the evaporation rate is low. Any remaining solution may then undergo a creeping mechanism and form crystals resembling efflorescence. Crystallization from solution can be divided into two steps. Forming new crystals is the first step, and their growth is the second;

the solution must be completely saturated<sup>24</sup>. At the end of the drying cycle, the hydrated crystals transform into an anhydrous shape with a different degree of opaque white colour. This gives a clear view of the film spreading around the droplet at the end of the evaporation process. It was observed that sodium chloride crystals formed more frequently when interacting with a nonpolar area (air or hydrophobic solid)<sup>25</sup>. When the pores absorb salt solutions, they cause fissures to form, and when they crystallize outside the body, the surface decorations are distorted. Rapid evaporation causes the growth of cubic-shaped salt crystals on the surface of the potsherds<sup>14</sup> (Figure 4).

The phenomenon acted in the presence of sodium chloride saline fog on excavated pottery sherd surfaces, dissolving water in the form of RH containing Na and Cl ions, followed by the crystallization of salt crystals during drying. The molecules in vapour form are dynamic, moving rapidly and spaced wide apart. They become slower, less energetic and come close together as the vapour comes into contact with decreasing air temperature. The vapour, which contains

ion salts, transforms into liquid drops when its energy level becomes low enough and stays in this condition for over 3–4 h. Then, with the rise in temperature, the salt drops turn to small and weak crystal salts (efflorescence) on the sherd surface; they appear in different degrees of intensity<sup>26</sup>. Condensation begins to appear on the surface of the pottery when the pores are saturated with steam to the point where it can no longer be tolerated. As the water molecules are too small to adhere to each other on their own, they need a surface or nucleation point for condensation<sup>27</sup>.

It is clear that the amount of salt crystallized is proportional to its concentration inside the pottery body. There is a direct and linear relationship between the salinity of the solution, its conductivity and the degree of crystallization<sup>26</sup>. From the following equations, the conditions for the growth of salt crystals under varying humidity and temperature conditions are consistent with the observed rates of rise in temperature and humidity in the environment surrounding the pottery sherd.

The well-known rate equations are as follows:

$$\frac{dq}{dt} = \text{Time rate of mass transport of water vapour to the droplet} = 4\pi D(R')^2 \left[ \frac{dp}{dR'} \right]. \quad (1)$$

$$\frac{dQ_1}{dt} = \text{Rate of heat transport away from the droplet} = 4\pi k(R')^2 \left[ \frac{dT}{dR'} \right]. \quad (2)$$

$$\frac{dQ_2}{dt} = \text{Rate of heat storage in the droplet} = mc_p \frac{dr}{dt} \frac{dT}{dt}. \quad (3)$$

where  $q$  is the quantity of water vapour (g),  $Q$  the quantity of heat (cal),  $dp/dR'$  the vapour density gradient ( $\text{g/cm}^3$ ),  $dT/dR'$  the temperature gradient ( $\text{K/cm}$ ),  $R'$  the radial distance (cm),  $D$  the diffusion coefficient of water vapour in air ( $\text{cm}^2/\text{sec}$ ),  $k$  the heat conduction coefficient of moist air ( $\text{cal cm}^{-1} \text{sec}^{-1} \text{deg}^{-1}$ ),  $c_p$  the specific heat of water at constant pressure ( $\text{cal g}^{-1} \text{deg}^{-1}$ ),  $T$  the temperature of droplet (deg),  $r$  the radius of droplet (cm),  $t$  the time (sec) and  $m$  is the mass of droplet (g).

The typical equations for temperature and vapour density gradients between the droplet radius  $r$ , and a point infinitely far from  $r$  are obtained by integrating eqs (1) and (2) over space. Additionally, it is assumed that the accommodation coefficient is taken to be unity and that the vapour that diffuses to the droplet condenses on it. Another presumption is that heat storage does not impact droplet growth, allowing for the approximation of  $dT/dr$  in eq. (3)<sup>28</sup>. Besides, capillary condensation (CC) is a frequently observed phenomenon

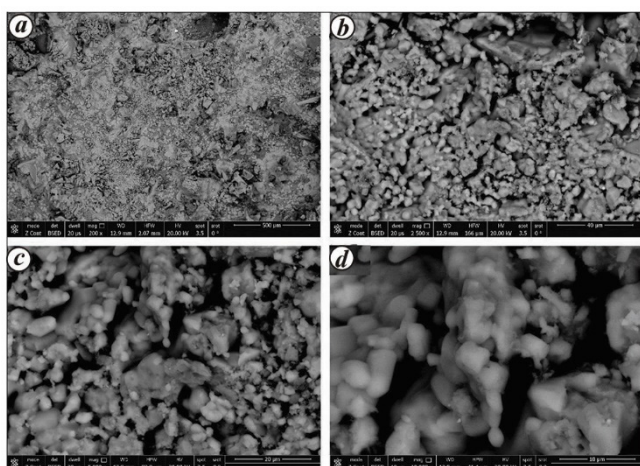


Figure 3. SEM photomicrographs of sample P1.

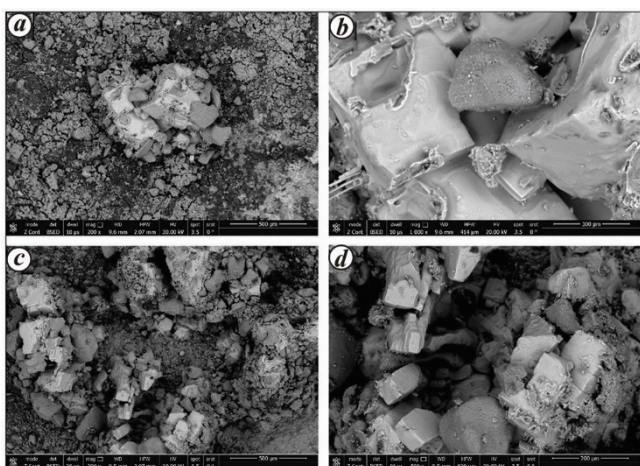
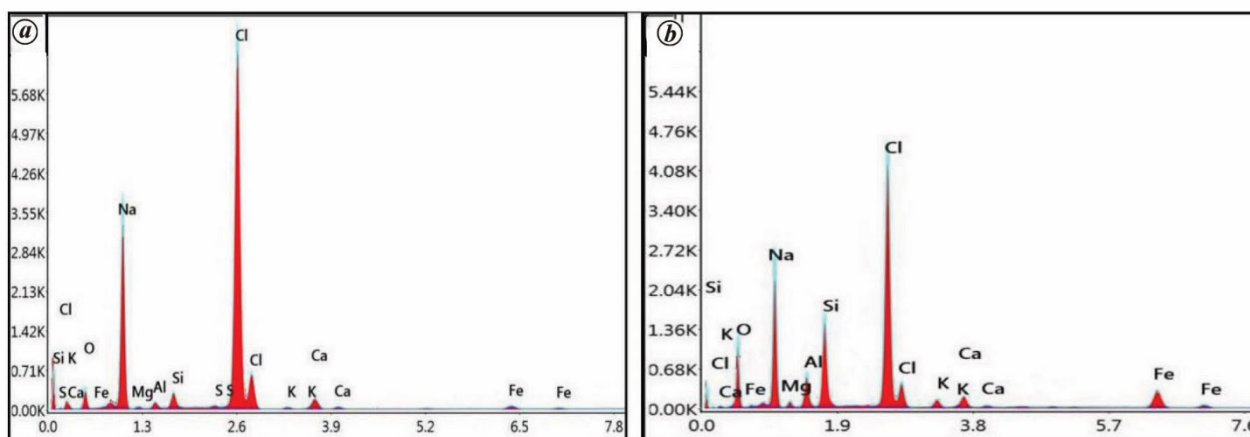


Figure 4. SEM photomicrographs of sample P2.

**Table 2.** Elemental concentration (wt%) of potsherd samples by SEM-EDX

Sample code	Elements									
	O	Na	Mg	Al	Si	S	Cl	K	Ca	Fe
P1	8.39	30.31	0.43	0.82	1.71	0.29	53.42	0.45	2.55	1.63
P2	19.18	22.98	0.8	3.74	8.63	—	32.8	1.4	2.9	7.57

**Figure 5.** SEM-EDX results: (a) Sample P1 and (b) sample P2.

characterized by the transformation of gas to liquid phase due to confinement, commonly occurring between the surfaces of particles or within porous materials<sup>29</sup>.

### SEM-EDX

EDX results from the samples revealed that they contained a high ratio of chloride salts, reaching 53.42% in the sample (P1) and 32.8% in the sample (P2) (Table 2 and Figure 5). In addition, sulphate salts were in minor proportion in sample P1 (0.29%). These findings indicate the presence of chloride and sulphate salts because of the burial of potsherds in a salty environment, resulting in several physio-chemical damages<sup>30</sup>. Furthermore, the aluminum and silica oxide ratio in the clay used to make the potsherds differs between samples. Besides, calcium oxide in the samples represents one of the clay additives used to make the potsherds. Based on the calcium oxide content in the pottery, noncalcareous and calcareous clay can be distinguished from one another<sup>31</sup>.

Calcium oxide helps improve the physical properties of the pottery, resulting in a high-quality product. CaO, SiO<sub>2</sub> and Al<sub>2</sub>O<sub>3</sub> react at temperatures above 800°C to form calcium silicate, such as diopside, which reveals a high firing temperature for pottery sherds<sup>32</sup>. The presence of hematite in the samples suggests that the potsherds were made in an oxidizing environment based on the availability of iron oxides<sup>33</sup>. The clay materials show a high SiO<sub>2</sub> ratio and moderate amounts of Al<sub>2</sub>O<sub>3</sub>, CaO and MgO. Additionally, the high SiO<sub>2</sub> ratio suggests that quartz minerals predomi-

nate over clay minerals, while a low K<sub>2</sub>O ratio indicates low illite content<sup>34</sup>.

### XRD

This is the most common method for analysing the crystalline structure of archaeological pottery<sup>35</sup>. XRD can determine the type of clay used in the industry of pottery, the firing impact, and the influence of the burial environment<sup>36</sup>. Table 3 and Figure 6 display the results of XRD analysis. The analysis indicates that the potsherd sample (P1) contains quartz, halite, diopside, hematite and magnetite. Quartz is one of the most common minerals in potsherds. It is also the main component in the pottery matrix<sup>37</sup>. Halite is present due to the strong effects of salt solution, crystals in the soil, and the rapid evaporation of water after excavation. Compared to materials with large pores, the crystallization compression of porous materials will be higher, and their interiors will primarily experience mineral precipitation (subflorescence). These two facts increase the likelihood that porous materials will deteriorate, lowering their resistance to crystallization<sup>13</sup>.

Diopside indicates a high firing temperature, as this compound is present at a temperature ranging from 850°C to 900°C. Furthermore, it indicates that the firing atmosphere is oxidizing. Additionally, hematite is a mineral element used as a colourant in the matrix of various pottery products and in the paint colours used to decorate the pottery surface, giving the material a reddish hue<sup>38</sup>. The XRD pattern

Table 3. XRD results for potsherd components

Sample code	Components (%)						
	Quartz	Diopside	Albite	Halite	Hematite	Muscovite	Magnetite
P1	50	12.4	–	28.9	5.3	–	3.4
P2	35.6	11	24.2	18.9	–	10.3	–

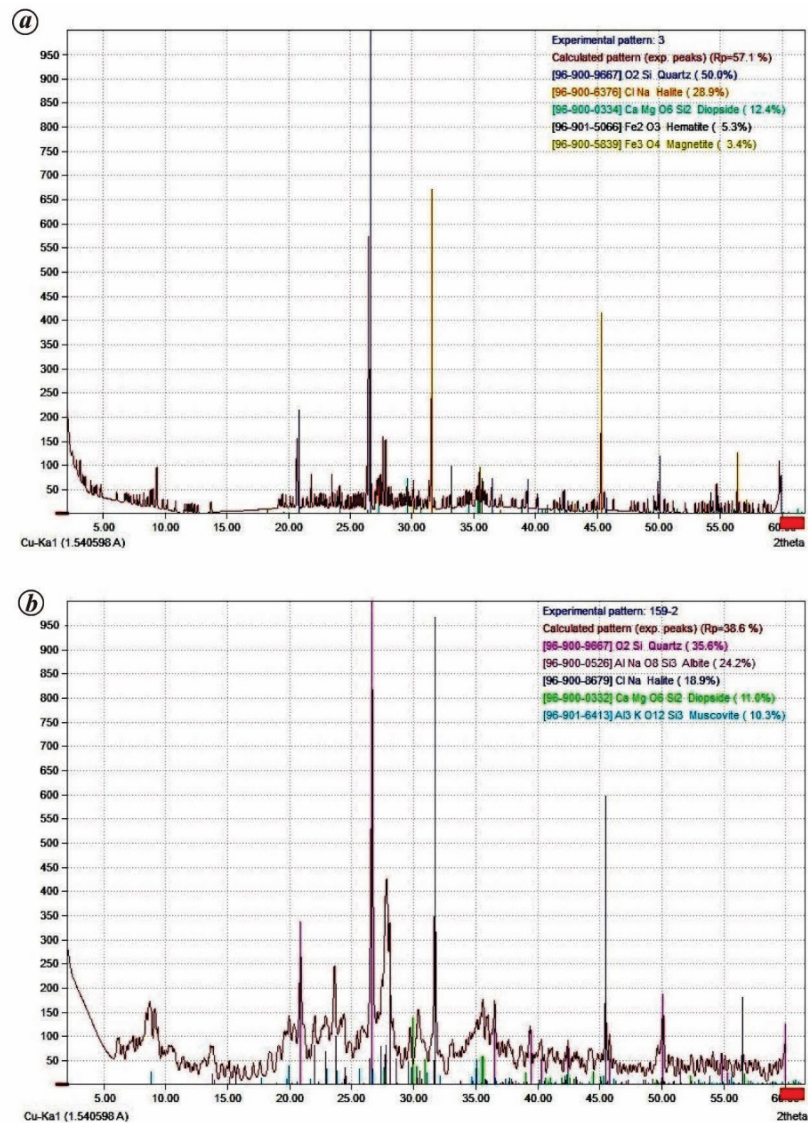


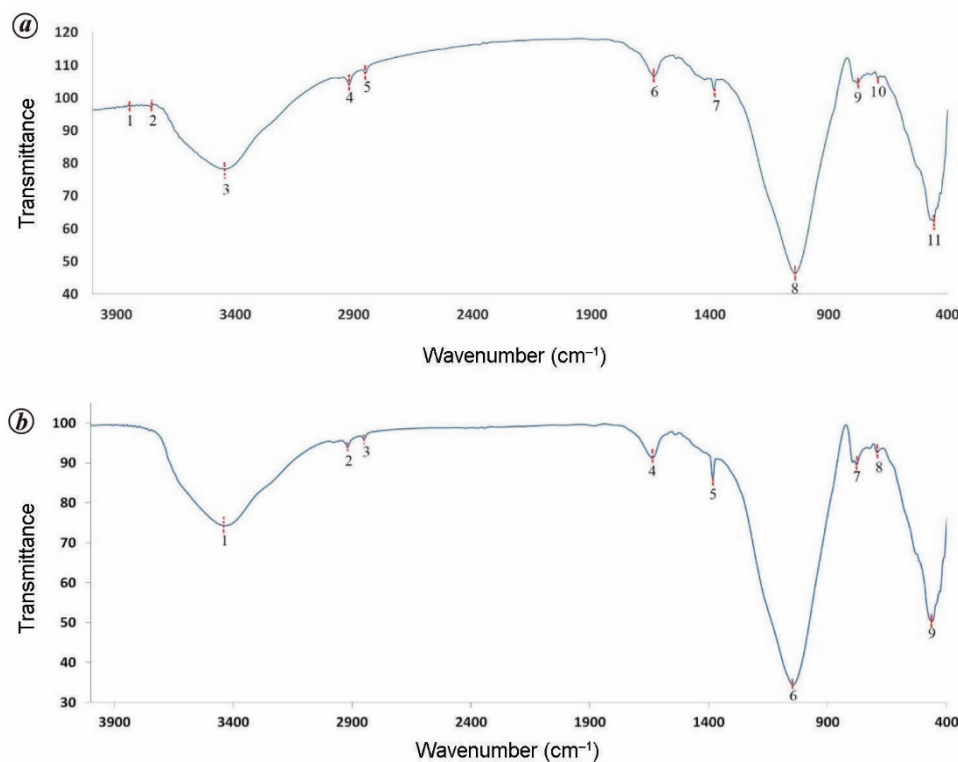
Figure 6. XRD patterns of potsherd samples: (a) Sample P1 and (b) sample P2.

shows that hematite makes up most of the reddish-brown pigment. Hematite formation starts at around 800°C, indicating that the firing atmosphere is oxidizing<sup>34</sup>. Magnetite is an iron oxide found in abundance in the core of the pottery<sup>3</sup>. XRD analysis shows sample P2 contains quartz, albite, halite, muscovite and diopside. The pottery sherds contain a medium proportion of silica, which is used as an additive material and forms a part of their mineral composition. Adding silica helps the water gradually evaporate from the

clay during pottery production, preventing the formation of cracks and imparting porosity to pottery<sup>39</sup>. Albite and muscovite are considered the main clay components used in pottery-making. Excess salt (NaCl) has been linked to several aspects of deterioration, as the local solution can migrate from the burial soil into the body of the pottery sherd. Rapid water evaporation can result in salt crystallization on the outer surface, which distorts the optical properties and hides the features of the archaeological

**Table 4.** FTIR results for potsherd components

Sample code	Wavenumber (cm <sup>-1</sup> )										
	1	2	3	4	5	6	7	8	9	10	11
P1	3841	3756	3436	2919	2851	1635	1383	1041	778	692	458
P2	3435	2918	2850	1638	1383	1045	778	692	458	—	—

**Figure 7.** FTIR bands of potsherds samples: (a) Sample P1 and (b) sample P2.

pottery<sup>33</sup>. Besides, most samples exhibit a red colour representing the outer slip layer due to the presence of iron minerals<sup>40</sup>. The iron oxide ratio (magnetite – Fe<sub>3</sub>O<sub>4</sub> and hematite – Fe<sub>2</sub>O<sub>3</sub>) in the samples reflects the oxidizing environment surrounding the firing process during industrial. The firing process was likely performed in a reducing atmosphere if the sample contained magnetite. If the sample contained hematite, the process was likely done in an oxidizing atmosphere<sup>34</sup>.

### FTIR

FTIR analysis was used to differentiate between various kinds of clay minerals. Additionally, the FTIR method enables quick identification of various clay minerals and permits observing structural changes due to chemical changes in clay minerals<sup>41</sup>. FTIR analyses on the two samples showed similarities in the chemical composition of the raw pottery clay (Table 4 and Figure 7). The range 4000–3000 cm<sup>-1</sup> can be attributed to water. The absorbed water from the

samples was also detected through obvious peaks from 3756, 3436 cm<sup>-1</sup> in sample P1, and 3435.56 cm<sup>-1</sup> in sample P2. This may result from the relative humidity of saline solution absorbed by halite or unfired clay found in the pottery core<sup>42</sup>. The FTIR spectra show an absorption band of clay at about 3435 cm<sup>-1</sup> that corresponds to H<sub>2</sub>O vibrations, indicating the ability of these materials to absorb water from the surrounding environment<sup>43</sup>.

The broadband spectrum of clay indicates the potential for water hydration in the adsorbent at 3436 and 1635 cm<sup>-1</sup> in sample P1 and 1638 cm<sup>-1</sup> in sample P2. Moreover, the presence of feldspar is indicated by splitting bands in the 800–400 cm<sup>-1</sup> region, including 778, 692 and 458 cm<sup>-1</sup> and one band at 1041 cm<sup>-1</sup> in samples P1 and P2. The absorption bands at 3435, 1045, 914, 778, 692 and 458 cm<sup>-1</sup> indicate the presence of kaolinite in all the samples<sup>44</sup>. Furthermore, the fired clay (meta-clay) is visible between 1032 and 1094 cm<sup>-1</sup>. Quartz is found in sample P1 at 778, 692 and 458 cm<sup>-1</sup> and in sample P2 at 778, 692 and 458 cm<sup>-1</sup>. Calcite is found in samples P1 and P2 at 1383 and 692 cm<sup>-1</sup> respectively. Moreover, the potsherds were

in contact with soil containing a high percentage of salts. Na, Cl and Ca concentrations were higher in the red area than in the black, incompletely fired parts<sup>45</sup>.

## Conclusion

This study describes the phenomenon of salt fog on the surface of potsherds from the Saqqara excavation. The microscopic analysis showed a thick distribution of salt on the potsherd surface and an overlap among the salt and sand layers scattered on the surface. Cubic crystals formed in the middle of low-concentration droplets. Moreover, when the evaporation rate of the salt solution is rapid, it leads to the formation of cubic salt crystals on the surface of the pottery. The findings of this study indicate that the interfacial characteristics influence where and how the crystals are formed. SEM-EDX results of the samples showed a high ratio of chloride salts, reaching 53.42% in sample P1 and 32.8% in sample P2. In addition, sulphate salts formed a minor proportion in sample P1 (0.29%). XRD analysis showed that both pottery samples contained salts, especially sodium chloride, but the percentage of salts in sample P1 was much higher than in sample P2. In addition, XRD and FTIR analyses confirmed the results of SEM-EDX in the presence of a large percentage of halite salt. These results helped properly diagnose crystallized salts on the archaeological potsherds. These findings will also help determine the most effective ways of extracting salts from archaeological pottery.

**Conflicts of interest:** The authors declare that they have no conflict of interest.

- Sáenz-Martínez, A., Pérez-Estébanez, M., Andrés, M. S., de Buergo M. A. and Fort, R., Efficacy of acid treatments used in archaeological ceramics for the removal of calcareous deposits. *Eur. Phys. J. Plus*, 2021, **136**, 1–16.
- Khalifa, E. and Abd Elrahim, E., Identification of vessel use and explanation of change in production techniques from the Old to the Middle Kingdom: organic residue analysis, fabric and thermal characterization of pot sherds from Qubbet el-Hawa, Aswan, Egypt. *Archaeometry*, 2020, **62**(6), 1115–1129.
- Ibrahim, M. M. and Mohamed, H. M., Analytical study and conservation of new kingdom period pottery jars from Saqqara excavation, Egypt. *Adv. Mater. Res.*, 2021, **1167**, 101–113.
- Wodzińska, A., *A Manual of Egyptian Pottery, Volume 3. Second Intermediate Period–Late Period*, Ancient Egypt Research Associates Inc, Boston, USA, 2010.
- Mohamed, H. M. and Mohamed, W. S., Evaluating nano Primal AC33 for protection and consolidation processes of archaeological pottery: a comparison study with silica and montmorillonite nanoparticles. *Pigm. Resin Technol.*, 2023; <https://doi.org/10.1108/prt-09-2022-0104>.
- Ibrahim, M. M., Mohamed, W. S. and Mohamed, H. M., Evaluation of the efficacy of traditional and nano Paraloid B72 for pottery consolidation. *Int. J. Conserv. Sci.*, 2022, **13**, 15–30.
- Sena da Fonseca, B. S., Simão, J. A. R. and Galhano, C., Effect of coastal environment in clay facing bricks and roof tiles. In First Annual International Interdisciplinary Conference, Azores, Portugal, 2013.
- Mohamed, H. M., Ahmed, N. M., Mohamed, W. S. and Mohamed, M. G., Advanced coatings for consolidation of pottery artifacts against deterioration. *J. Cult. Herit.*, 2023, **64**, 120–135.
- Lubelli, B., Hees, R. P. J. and Groot, C. J. W. P., Sodium chloride crystallization in a ‘salt transporting’ restoration plaster. *Cem. Concr. Res.*, 2006, **36**, 1467–1474.
- Angeli, M., Hébert, R., Menéndez, B., David, C. and Bigas, J. P., Influence of temperature and salt concentration on the salt weathering of a sedimentary stone with sodium sulphate. *Eng. Geol.*, 2010, **115**, 193–199.
- Di Benedetto, C., Cappelletti, P. and Favaro, M., Porosity as key factor in the durability of two historical building stones: Neapolitan Yellow Tuff and Vicenza Stone. *Eng. Geol.*, 2015, **193**, 310–319.
- Angeli, M., Benavente, D., Bigas, J. P., Menendez, B., Hebert, R. and David, C., Modification of the porous network by salt crystallization in experimentally weathered sedimentary stones. *Mater. Struct.*, 2008, **41**, 1091–1108.
- Benavente, D., Garcia del Cura, M. A., Garcia-Guinea, J., Sanchez-Moral, S. and Ordóñez, S., Role of pore structure in salt crystallisation in unsaturated porous stone. *J. Cryst. Growth*, 2004, **260**, 532–544.
- Zornoza-Indart, A., López-Arce, P., Simão, J., Leal, N. and Zoghalmi, K., Accelerated aging experiments with saline fog, involving ventilation in calcarenitic monument rocks. *Commun. Geol.*, 2014, **101**, 1181–1185.
- Scrivano, S. and Gaggero, L., An experimental investigation into the salt-weathering susceptibility of building limestones. *Rock Mech. Rock Eng.*, 2020, **53**, 5329–5343.
- Ottosen, L. M., Pedersen, A. J. and Rorig-Dalgaard, I., Salt-related problems in brick masonry and electrokinetic removal of salts. *J. Build. Apprais.*, 2007, **3**(3), 181–194.
- Silva, Z. S. G. S. and Imão, J. A. R., The role of salt fog on alteration of dimension stone. *Constr. Build. Mater.*, 2009, **23**, 3321–3327.
- Quilaqueo, M. and Aguilera, J. M., Crystallization of NaCl by fast evaporation of water in droplets of NaCl solutions. *Int. Food Res. J.*, 2016, **84**, 143–149.
- Cardell, C., Delalieux, F., Roumpopoulos, K., Moropoulou, A., Auger, F. and Van Grieken, R., Salt-induced decay in calcareous stone monuments and buildings in a marine environment in SW France. *Constr. Build. Mater.*, 2003, **17**, 165–179.
- Bracciale, M. P., Sammut, S., Cassar, J., Santarelli, M. L. and Marrocchi, A., Molecular crystallization inhibitors for salt damage control in porous materials: an overview. *Molecules*, 2020, **25**, 1873.
- Mohamed, H. M., Study and characterization of Old Kingdom period potsherds from Abusir excavation. A case study. *J. Sci. Arts*, 2022, **22**(3), 723–734.
- Naillon, A., Duru, P., Marcoux, M. and Prat, M., Evaporation with sodium chloride crystallization in a capillary tube. *J. Cryst. Growth*, 2015, **422**, 52–61.
- Çelik, M. Y. and Aygün, A., The effect of salt crystallization on degradation of volcanic building stones by sodium sulfates and sodium chlorides. *Bull. Eng. Geol. Environ.*, 2019, **78**, 3509–3529.
- Vázquez, P. et al., Infrared thermography monitoring of the NaCl crystallisation process. *Infrared Phys. Technol.*, 2015, **71**, 198–207.
- Shahidzadeh-Bonn, N., Rafai, S., Bonn, D. and Wegdam, G., Salt crystallization during evaporation. *Langmuir*, 2008, **24**, 8599–8605.
- Feliciano, I., *Cerâmica Arqueológica: estudo comparativo da eficácia de consolidantes aplicados no processo de dessalinização*. Dissertação para obtenção do grau de Mestre em Conservação e Restauro, Faculdade de Ciências e Tecnologia (FCT) FCT Departamentos FCT: Departamento de Conservação e Restauro FCT, DCR, Universidade de Lisboa, Portugal, 2016.
- Broström, M., Enestam, S., Backman, R. and Mäkelä, K., Condensation in the KCl–NaCl system. *Fuel Process. Technol.*, 2013, **105**, 142–148.
- Keith, C. H. and Arons, A. B., The growth of sea salt particles by condensation of atmospheric water vapor. *J. Atmos. Sci.*, 1954, **11**, 173–184.

29. Yarom, M. and Marmur, A., Capillary condensation with a grain of salt. *Langmuir*, 2017, **106**, 13444–13450.
30. Mohamed, H. M., A comparison study of titanium dioxide and zinc oxide nanoparticles for cleaning archaeological pottery. *J. Nano Res.*, 2022, **76**, 61–77.
31. Tite, M. S., Pottery production, distribution, and consumption – the contribution of the physical sciences. *J. Archaeol. Method Theory*, 1999, **6**(3), 181–233.
32. Grammatikakis, I. E., Kyriakidis, E., Demadis, K. D., Diaz, A. C. and Leon-Reina, L., Mineralogical characterization and firing temperature delineation on Minoan pottery, focusing on the application of micro-Raman spectroscopy. *Heritage*, 2019, **2**, 2652–2664.
33. Olivares, M. *et al.*, Characterisation of fine wall and eggshell Roman pottery by Raman spectroscopy. *J. Raman Spectrosc.*, 2010, **41**, 1253–1259.
34. Kiliç, N. Ç., Kiliç, S. and Akgül, H. Ç., An archaeometric study of provenance and firing technology of Halaf pottery from Tilkitepe (Eastern Turkey). *Mediterr. Archaeol. Archaeom.*, 2017, **17**(2), 35–48.
35. Poppe, L. J., Paskevich, V. F., Hathaway, J. C. and Blackwood, D. S., *A Laboratory Manual for X-Ray Powder Diffraction*, US Geological Survey Open-File Report 01-041, 2001.
36. Abd Elrahim, E. and Weshahy, I., The mortar damage and its harmful effects on the glazed ceramic tiles in Terbana Mosque–Alexandria, Egypt. *Shedet*, 2017, **4**, 155–166.
37. Abd-Allah, R., Al-Muheisen, Z. and Al-Howadi, S., Cleaning strategies of pottery objects excavated from Khirbet Edh-Dharih and Hayyan Al-Mushref, Jordan: four case studies. *Mediterr. Archaeol. Archaeom.*, 2010, **10**(2), 97–110.
38. De Nolf, W., Dik, J., Vandersnickt, G., Wallert, A. and Janssens, K., High-energy X-ray powder diffraction for the imaging of (hidden) paintings. *J. Anal. At. Spectrom.*, 2011, **26**, 910–916.
39. Velde, B. and Durc, I. C., *Archaeological Ceramic Materials: Origin and Utilization* (eds Herrmann, B. and Wagner, G. A.), Natural Science in Archaeology, Springer-Verlag Berlin Heidelberg, 1999.
40. Al-Naddaf, M., Provenance and firing technology of Iron Age pottery of Tell Johfiyeh, northern Jordan, Yarmouk University. *J. Yarmouk Univ.*, 2006, **22**(4), 149–165.
41. Madejova, J., FTIR techniques in clay mineral studies. *Vib. Spectrosc.*, 2003, **31**, 1–10.
42. Drob, A., Vasilache, V. and Bolohan, N., The interdisciplinary approach of some Middle Bronze Age pottery from Eastern Romania. *Appl. Sci.*, 2021, **11**, 4885.
43. Nayak, P. S. and Singh, B. K., Instrumental characterization of clay by XRF, XRD and FTIR. *Bull. Mater. Sci.*, 2007, **30**, 235–238.
44. Jozanikohan, G. and Abarghoeei, M. N., The Fourier transform infrared spectroscopy (FTIR) analysis for the clay mineralogy studies in a clastic reservoir. *J. Pet. Explor. Prod. Technol.*, 2022, **12**, 2093–2106.
45. Vasilache, V., Kavruk, V. and Tencariu, F., OM, SEM-EDX, and micro-FTIR analysis of the Bronze Age pottery from the Baile Figa salt production site (Transylvania, Romania). *Microsc. Res. Tech.*, 2020, **83**, 604–617.

**ACKNOWLEDGEMENTS.** We thank Prof. Dr Ola El-Augizi (Faculty of Archeology, Cairo University, Egypt) for her assistance and encouragement during this study. We also thank Prof. Dr Tariq Tawfiq, Dr Nader Elhosiny, Magdi Al-Beheiri, Montasir Kamal and Weaam Ashour for help.

Received 13 March 2023; revised accepted 6 September 2023

doi: 10.18520/cs/v126/i1/85-93